Structural transformations of bioactive glass 45S5next term with thermal treatments

Leila Lefebvre, Jérome Chevalier, Laurent Gremillard, Rachid Zenati, Gilbert Thollet, Didier Bernache-Assollant, Alexandre Govin

Acta Materiala, 2007, 55(10), 3305-3313, doi:10.1016/j.actamat.2007.01.029

Structural transformations of bioactive glass 45S5 with thermal treatments

LEFEBVRE, LEILA[(1)] ; CHEVALIER, JÉRÔME[(1)] ; GRÉMILLARD, LAURENT[(1)*] ; ZENATI, RACHID[(2)] ; THOLLET, GILLES[(1)], BERNACHE-ASSOLLANT, DIDIER[(3)] ; GOVIN, ALEXANDRE[(4)]

(1) *MATEriaux, Ingénierie et Sciences (MATEIS) CNRS : UMR5510 – Institut National des Sciences Appliquées de Lyon*
(2) *Noraker, 13, avenue Albert Einstein - 69100 Villeurbanne - France*
(3) *Ecole Nationale Supérieure des Mines de Saint Etienne, Centre CIS ; Département DBM ; 158 Cours Fauriel ; 42023 Saint-Étienne Cedex 2, France*
(4) *Ecole Nationale Supérieure des Mines de Saint Etienne, Centre SPIN ; Département PMMC ; 158 Cours Fauriel ; 42023 Saint-Étienne Cedex 2, France*

Abstract
We report on the structural transformations of Bioglass® during thermal treatments. Just after the glassy transition, at 550 °C, a glassy phase separation occurs at 580 °C, with the appearance of one silicate- and one phosphate-rich phase. It is followed by the crystallization of the major phase $Na_2CaSi_2O_6$, from 610 to 700 °C and of the secondary phase, silico-rhenanite, at 800 °C. The latter evolves from the phosphate-rich glassy phase, which is still present after the first crystallization. In order to control the processing of glass-ceramic products from Bioglass®, crystallization kinetics were studied via differential scanning calorimetry measurements in the range of 620–700 °C and temperature–time–transformation curves were established.

Keywords:

Silicates; Bioactive glasses; Crystallization; Differential scanning calorimetry; X-ray diffraction

I. Introduction
Bioactive glasses are biocompatible and exhibit a strong interfacial bonding with bone. Their bioactivity is attributed to the formation on their surface of a hydroxycarbonated apatite (HCA) layer similar to a large extent to the mineral part of bone. The rate of tissue bonding appears to depend on the rate of HCA formation, which follows a sequence of reactions between the implanted material and the surrounding tissues and physiologic fluids [1]. Hench *et al.* [2] proposed a three-step mechanism of HCA formation when the bioactive glass comes into contact with physiologic fluids: ion exchange, dissolution and precipitation. Ion exchange occurs at the bioactive glass surface: cations such as Na^+ and Ca^{2+} from the glass exchange with H^+ from the surrounding solution. Network dissolution occurs from the breakage of Si–O–Si bonds by the action of hydroxyl ions (OH^-). The hydrated silica (SiOH) formed on the glass surface undergoes rearrangement by polycondensation of neighbouring silanols, resulting in a silica-rich gel layer. Precipitation of the calcium and phosphate ions released from the glass together with those from the solution form a calcium–phosphate-rich layer (CaP) on the surface. The reactions involved in this process were observed by several authors

* Auteur à qui la correspondance devait être adressée Laurent.gremillard@insa-lyon1.fr

in vitro as well as in vivo [3], [4] and [5]. The study of different compositions in the ternary Na_2O, SiO_2, CaO system with 6 wt.% P_2O_5 showed that the 45S5 Bioglass® (45 wt.% SiO_2, 24.5 wt.% Na_2O, 24.5 wt.% CaO, 6 wt.% P_2O_5) is the most bioactive glass. It is nowadays used successfully as middle ear and dental implants [6].

The poor mechanical strength of bioactive glasses is a major problem that limits their application as load-bearing implants. Approaches to achieve enhanced mechanical and biochemical properties include transformation of bioactive glasses into glass-ceramic. In this technique, the glasses are subjected to thermal treatments which may affect the materials microstructures and hence their mechanical properties, but also their biological activity.

Most of the existing literature on the transformation of 45S5 Bioglass® shows that thermal treatments above 600 °C result in the formation of $Na_2Ca_2Si_3O_9$ as the main crystalline phase [7], [8], [9], [10], [11] and [12]. A secondary minor phase, $Na_2CaSi_3O_8$, is often suggested to match the stoichiometry of the initial glass [13]. For some authors [14], raising the temperature to 800 °C for a long period leads to the development of calcium phosphate crystals with a structure similar to hydroxyapatite. However, the real composition of the crystals appearing during thermal treatments of Bioglass® still remains unclear. As an example, Lin *et al.* [15] proposed $Na_2CaSi_2O_6$ rather than $Na_2Ca_2Si_3O_9$ to be the major crystalline phase. Moreover, to our knowledge, there is no detailed investigation on the lattice parameters of the proposed crystalline phases and their evolution versus temperature. In addition, the location of phosphorous ions in the structure and its influence on the transformation processes is still not understood.

45S5 Bioglass® has the potential to be used in many more bioactive applications than hydroxyapatite. Our global strategy is therefore to extend the application fields of 45S5 Bioglass® by the processing, from powders, of porous blocks for bone substitution applications and tissue engineering [16]. This necessitates the optimization of the mechanical and biological properties of porous bioactive glasses via a careful understanding of the process–microstructure–biomechanical properties relations. In particular, it is crucial to control bioactivity and mechanical properties by a full knowledge of microstructural evolutions during thermal treatments. The aim of the present paper is therefore to provide a precise understanding of the major transformation processes occurring during thermal treatment of Bioglass® and to control the major phase crystallization kinetics via temperature–time–transformation (TTT) curves.

II. Materials and methods

II.1. Bioglass® preparation

High purity SiO_2, Na_2CO_3, $CaCO_3$ and P_2O_5 powders were weighted and mixed to obtain 45S5 Bioglass® (45 SiO_2, 24.5 CaO, 24.5 Na_2O, 6 P_2O_5 in wt.%). The powders were melted in a Pt crucible for 4 h at 1400 °C with a decarbonatation step (5 h at 950 °C). The melt was then quenched in water and ground in ethanol to a fine powder (1 µm). Quenching was fast enough to retain a completely amorphous material, as verified by X-ray diffraction (XRD). The composition was also checked by chemical analysis, to ascertain that no impurity was present after the different preparation steps.

II.2. Transformations processes

II.2.1 In situ follow-up

The transformations of the glass powder were followed with two methods:

- Simultaneous thermal gravimetric analysis–differential thermal analysis (TGA–DTA; SETARAM TG-DTA 92, Caluire, France) on powders, for which 20 mg of powder was heated in a 20% N_2–80% O_2 atmosphere at 5 °C min^{-1} up to 1300 °C.
- Environmental scanning electron microscopy (ESEM; FEI, XL30, Eindhoven, Netherlands), with an in situ heating stage. In order to get an easier observation, larger grains (on the order of 10 µm) were introduced into a Pt crucible. They were heated up

to 950 °C (heating rate 5 °C min⁻¹) in the microscope. Measurements were conducted with a 1.9 Torr (250 Pa) water pressure.

II.2.2 Characterization of thermally treated powders

Several thermal treatments for 5 min (heating rate 5 °C min^{-1}) in the range of 550–950 °C were carried out on the glass powder. Two types of investigations were then performed:

- XRD (RIGAKU vertical diffractometer, Kent, UK), to identify the crystalline phases and their evolution versus temperature. Samples were obtained by pressing a mixture of 45S5 Bioglass® powder with an amorphous binder (PEG 1500) into 1 cm diameter pieces. These pieces were then analysed with Cu Kα radiations from $2\theta = 10°$ to $2\theta = 90°$ at 2° min^{-1} for the crystalline phases determination and 0.2° min^{-1} for Rietveltd analysis and crystallite size calculation. The crystallite size of the main phase, $Na_2CaSi_2O_6$, at the different temperatures was estimated via the Scherrer equation on the peaks of higher intensity ($2\theta \cong 34°$)

$$\beta = \frac{k.\lambda}{\varsigma.\cos\theta} \tag{1}$$

  where β is the full width at half maximum of the peak, ς is the crystallite size in meters, λ the wavelength of the Cu Kα line (1.5406×10^{-10} m) and k is the Scherrer constant equal to 0.89. Rietveltd analysis was performed with the software WINPLOTR® to evaluate the lattice parameters of the main phase. The diffractograms conducted at different temperature were compared with theoretical diffractograms of $Na_2CaSi_2O_6$ established from the structure determined by Oshato and Maki [17].

- Fourier transformed infrared analysis (FTIR; Nicolet Magna-IR 550 spectrometer, Madison, Wisconsin) was performed to identify the nature of the chemical bonds between atoms. The samples were small pellets, of 0.5 cm diameter, obtained by pressing the glass powder with KBr.

II.3. Crystallization kinetics: TTT curves

The crystallization kinetics of the major phase were investigated by differential scanning calorimetry (DSC). Several isothermal measurements were conducted between 620 and 680 °C on 10 mg of powder. The samples were subjected to a first heating until 460 °C at 15 °C min−1, followed by a plateau of 15 min in order to stabilize the temperature and a second heating at 50 °C min−1 to the desired temperature. The samples were then held for 90 min at the isothermal temperature. The total area of exothermic crystallization peaks was measured for each temperature. The area of the peak at each time for a given temperature normalized by the total area was calculated. These results allow the determination of a degree of transformation for a given time and a given temperature, *i.e.* TTT curves. The degree of transformation at a given time for a given temperature, $\alpha_T(t)$, was calculated from the following expression:

$$\alpha_T(t) = \left(\frac{\int_0^t H_f(t).dt}{\int_0^{t_f} H_f(t).dt} \right)_T \tag{2}$$

where H_f is the heat flow, t the time and t_f the duration of the dwell at a given temperature (*i.e.* 90 min).

III. Results

III.1. In situ follow-up of transformation processes

Figure 1 shows the TGA–DTA curve. TGA shows a total 2.8% weight reduction, which can be divided in two main weight losses, at 100 and 400 °C. They are due respectively to the departure of free water and –OH groups. The small apparent weight loss at 610 °C may be attributed to the onset of crystallization. DTA shows an endothermic effect at T_{g1} = 550 °C caused by the glass transition, followed by an exothermic peak beginning at T_{c1} = 610 °C. These two events were already well identified in the literature [7], [9] and [14]. A second small endothermic effect is observed at T_{g2} = 850 °C. This event had already been observed [9] and [14] but not discussed in the existing literature. Finally, melting takes place in the 1070–1278 °C range. Two endothermic peaks (maximum signal respectively at T_{m1} = 1192 °C and T_{m2} = 1235 °C) may be attributed to the melting of two different crystalline phases.

Figure 2 shows ESEM micrographs taken at low magnification on one Bioglass® grain during in situ heating from room temperature to 950 °C. Three micrographs have been selected to show the evolution of grain morphology with temperature: 110 °C (similar to the morphology at room temperature) (Figure 2a), around T_{g1} = 550 °C (Figure 2b) and around T_{g2} = 850 °C (Figure 2c). These micrographs show two steps of particle rounding at T_{g1} and T_{g2}. Between T_{g1} and T_{g2} the rounding of the particles seems to slow down. These two temperatures must therefore correspond to two glassy transitions.

Figure 3 shows ESEM micrographs taken in situ at higher magnification at the surface of the same grain. Figure 3a, taken below the glass transition (T_{g1}), exhibits the features of a faceted ground powder. Figure 3b, taken at T_{g1} = 550 °C, shows a significant modification of its morphology. The grain is more rounded, confirming the glassy transition. An additional event is observed at T_s = 570 °C (Figure 3c), prior to crystallization, which was not observed on the DTA thermograms: the surface, which was completely smooth after the glassy transition, presents a specific morphology, with the creation of domains. This may be attributed to the glass-in-glass phase separation expected when two high valence ions such as Si^{4+} and P^{5+} are present simultaneously in a glass [18] and [19]. Each ion type tends to concentrate in a separate phase. Figure 3d, taken at 700 °C, shows the result of crystallization, with the formation of ‘craters’ at the surface. At 800 °C, Figure 3e shows the migration of a second phase with a different morphology and structure. The present micrograph was obtained via charge contrast imaging, which relates to electrical conductivity variations in the sample. The last figure, Figure 3f, shows the resulting surface after thermal treatment at 950 °C (the micrograph was taken at ambient temperature, after cooling, to ensure thermal stability and better contrast and resolution). On this micrograph, the separation between the two types of domain is still more pronounced, with a spinodal like morphology. Large crystals (about 500 nm diameter) are observed. They may be attributed to a heterogeneous grain growth at high temperature (Ostwald ripening).

III.2. Characterization of thermally treated powders

Figure 4 shows the X-ray diffractograms of the powder before and after thermal treatments between 550 and 950 °C. The results obtained for the powder before any treatment confirm the amorphous nature of Bioglass® after quenching and grinding. Crystallization is observed at 600 °C, which is in agreement with the results obtained by TGA–DTA analysis. The crystalline phase is identified as $Na_2CaSi_2O_6$ rather than $Na_2Ca_2Si_3O_9$, as shown previously by Lin *et al.* [15]. An apparent broadening of the main peak (at 2θ = 33.75°) occurs at 750 °C; this is in fact the beginning of the separation into two peaks, still both attributed to $Na_2CaSi_2O_6$. The separation is clearly observed at 800 °C and intensifies at higher temperatures. Concurrently, in the 800–950 °C range, a new small peak is observed (arrow), suggesting that a secondary crystalline phosphate phase appears. This peak was attributed to silicorhenanite ($Na_2Ca_4(PO_4)_2SiO_4$).

In order to understand the separation of the two main peaks, more precise XRD analyses (at lower scan speed and better angular resolution) were performed on powders treated between 750 and 950 °C. The diffractogram between 33° and 34.5° was fitted by two pseudo-Voigt functions, and the distance between the two peaks calculated for each temperature. Figure 5 shows the separation of these two peaks ($\Delta 2\theta$) as a function of temperature. A linear dependency is observed. Thus it can be inferred that the peak separation is due to a variation of lattice parameters rather than to a phase change. A Rietveltd refinement was applied to the different diffractograms to measure the lattice parameters (a and c). The evolution is represented in Figure 6. The figure shows that a decreases gradually with temperature, while a steep increase of *c* is noticed around 800 °C, when the secondary phase appears. Table 1 summarizes the $Na_2CaSi_2O_6$ crystal size evaluated from XRD, calculated via Equation (1). It varies from 15 to 41 nm between 650 and 950 °C.

FTIR spectra taken on the powder before and after thermal treatments at 800 °C are shown in Figure 7. The main absorption bands for the amorphous Bioglass® are observed at 1024, 926 and 480 cm^{-1}. They are commonly attributed to Si–O–Si and Si–O stretching modes and Si–O–Si bending mode, respectively. These bands are generally observed in amorphous silica glasses [20] and [21]. The band at 600 cm^{-1} is related to amorphous phosphate. The FTIR spectra of the powder treated at 800 °C shows that the broad band at 1024 cm^{-1} is split into two bands due to the combination of isolated tetrahedral Si. At the same time, the band at 926 cm^{-1}, which is attributed to the Si–O bond with non-bonding oxygen, increases in intensity. This increase is due to the crystallization of the major phase $Na_2CaSi_2O_6$ [12], in agreement with XRD data. The presence of a crystalline calcium phosphate (apatite like) phase is suggested by the new bands at 620, 580 and 530 cm^{-1} since the dual peaks at about 620 and 580 cm^{-1} are attributed to P–O bending vibration [14]. This is also in agreement with XRD and the identification of the silicorhenanite phase.

III.3. Crystallization kinetics: TTT curves

Few papers report on the crystallization kinetics of bioactive glasses [22], [23] and [24]. In particular, TTT curves on bioactive glass 45S5 have never been established, although this type of curve can serve as a basis for the elaboration and thermal treatments of porous blocks. Crystallization isotherms were conducted between 620 °C (onset of $Na_2CaSi_2O_6$ crystallization) and 680 °C (to avoid the apparition of the secondary phase). DSC measurements made on the isothermal plateau at temperature in the 620–680 °C range (Figure 8) show exothermic peaks of crystallization. As expected when a single transformation mechanism is involved in a given range of temperature, the peak intensity increases with temperature, while the area of the peak remains constant. The enthalpy of crystallization is given by the area of the peaks, and is found to be constant (84 ± 10 J g^{-1}), independent of temperature. The plot of $\alpha_T(t)$ vs. time obtained from the DSC measurements and from Equation (2) is given in Figure 9. The knowledge of the degree of transformation ($\alpha_T(t)$) calculated at given times and temperatures allows the plotting of TTT curves in Figure 10.

The kinetics of Bioglass® crystallization have been previously analysed using methods based on the Avrami equation [8]

$$\alpha_T(t) = 1 - \exp(-(bt)^n) \tag{3}$$

where *b* is given by the Arrhenius relation:

$$b = b_0.\exp\left(-\frac{Q}{RT}\right) \tag{4}$$

where b_o is a constant, *Q* the activation energy and *R* the gas constant. The Avrami exponent is generally obtained by plotting $\ln\left(\ln\left(\frac{1}{1-\alpha}\right)\right)$ as a function of ln(*t*) and the apparent activation energy given by the plot of ln(*b*) vs. $\frac{1}{T}$. Figure 11 summarizes the values obtained for *n* and ln(*b*) for each temperature. In agreement with the study of Clupper and Hench [8], conducted with non-isothermal kinetics, the mean value of *n* (about 1) is consistent with a slow nucleation on the surface and infinitely rapid growth of the nuclei, and the apparent activation energy is close to 280 kJ mol^{-1}.

IV. Discussion and summary of the structural transformations occurring in Bioglass® 45S5

The different observations conducted on Bioglass® with various techniques allow us to propose a possible scenario of the structural transformations occurring during thermal treatments from room temperature to 950 °C. The first step is the glass transition around $T_{g1} = 550$ °C, which has already been reported extensively in the literature. It is followed by a glass-in-glass phase separation at $T_s = 570$ °C. This means that the glass is no longer homogeneous but rather consists of two immiscible phases. The viscosity of a phase-separated silicate glass is usually higher than that of a homogeneous glass of the same composition because of the high viscosity of the silica-rich phase that dominates flow behaviour [19]. This is consistent with our ESEM observations, which shows that the rounding of the particles starting at $T_{g1} = 550$ °C seems to slow down around $T_s = 570$ °C, indicating a decrease of mobility in the material. The formation of phosphate-rich domains during the glass-in-glass phase separation should have a catalytic effect on the nucleation of the major crystalline phase at $T_{c1} = 610$ °C as they decrease the necessary energy for nucleation of the surrounding silicate-rich nuclei (the phosphate-rich domains may act as heterogeneous nucleation sites). The Avrami exponent of about 1 is consistent with a predominant slow nucleation on the surface and infinitely rapid growth of the nuclei, in accordance with Clupper and Hench [8]. The major crystalline phase, appearing at $T_{c1} = 610$ °C, is identified by XRD as $Na_2CaSi_2O_6$ rather than $Na_2Ca_2Si_3O_9$, as shown previously by Lin *et al.* [15]. $Na_2CaSi_2O_6$ is isostructural to the high temperature form of $Na_2Ca_2Si_3O_9$ (2 Na replace 1 Ca ion), which could explain why 45S5 was thought to crystallize in the $Na_2Ca_2Si_3O_9$ phase [25]. Two arguments are in favour of $Na_2CaSi_2O_6$ rather than $Na_2Ca_2Si_3O_9$. First, the composition of Bioglass® is closer to $Na_2CaSi_2O_6$. Second, the Rietveldt analysis shows a better agreement of the experimental diffraction pattern with that calculated for $Na_2CaSi_2O_6$. However, a complete determination of the crystalline structure, including positions of the atoms and taking into account the possible solid solution, is still lacking. The $Na_2CaSi_6O_{16}$ phase mentioned in other studies was not observed in our material. The crystallization mechanism of the major phase in Bioglass® is in agreement with the results of Koga *et al.* [26], who studied the mechanism of crystallization in the Na_2O–CaO–$2SiO_2$ system leading to $Na_2CaSi_2O_6$ and found that a surface nucleation takes place for small particles (*i.e.* smaller than 100 µm).

El Ghannam *et al.* [9] found that the change in bioactive glass microstructure after crystallization alters the corrosion behaviour by accelerating the dissolution kinetics of phosphorus in physiological fluid and slowing the Na and Ca dissolution. This also led to a significant increase in the zeta potential of the material. In conjunction with this increase, they observed a significant decrease in the amount of serum protein adsorbed onto the material surface. On the other hand, crystallization is beneficial for the mechanical properties and helps tailor the dissolution kinetics to the bone growth rate.

In the 800–950 °C range, a secondary phosphate phase crystallizes. It is identified in X-ray diffractograms as silicorhenanite ($Na_2Ca_4(PO_4)_2SiO_4$). This phase is isostructural to apatite and was never identified in Bioglass® after short thermal treatments at 800 °C. Lin *et al.* [15] showed by Raman analysis that in the 45S5 glass, phosphorus has the same behaviour than in pure silica. It tends to depolymerize the silicate network by entering the network as a fourfold-coordinated cation. However, McMillan [27] thought that the double oxygen/phosphorus (P═O) bond is favourable to phosphate phase formation in a silica network and thus increases the tendency towards crystallization. Elgayar *et al.* [28] showed by nuclear magnetic resonance of phosphorus analysis applied to the 45S5 glass that 75% of the phosphorous ions are in an orthophosphate (PO_4^{3-}) environment, while 25% are under the form of a diphosphate specie ($P_2O_7^{4-}$). Using the relative XRD intensity peaks, we found around 4% of phosphate crystalline phase. This indicates that 75% of phosphorus ions in the material are in the crystalline phosphate phase. This is consistent with the fact that in silicorhenanite, phosphorus is in the orthophosphate form. Thus we concluded that the orthophosphate ions in the glass lead to the formation of the crystalline phase whereas the diphosphate species remain in the amorphous phase. The significant increase of the cell parameter *c* around 800 °C is attributed to a departure of orthophosphate in insertion in the silica network and to the replacement of these groups by SiO_4 groups. The orthophosphate species would then form the crystalline phosphate phase.

After nucleation of the principal crystalline phase, differential grain growth leads to an Oswalt ripening, where only big crystallites can grow at the expense of smaller crystallites. Then, a migration of the phosphate vitreous phase around the bigger crystallites of $Na_2CaSi_2O_6$ takes place. We can imagine that the new interface formed has a catalytic effect on the crystallization of the phosphate phase *(i.e.* the $Na_2CaSi_2O_6$ surface acts as nucleation site for silicorhenanite).

Höland *et al.* [29] studied the influence of rhenanite crystallization in bioactive glasses (containing, in wt.%, 6 P_2O_5, 58 SiO_2, 22.8 Na_2O, 12.9 CaO and 0.3 F) on the crystallization of carbonated hydroxyapatite on their surface. They concluded that this phase acts as heterogeneous nuclei for HCA crystallization and thus should improve the bioactivity. On the other hand, the state of phosphorus ions affects the bioactivity: glass ceramics containing a crystalline phosphate phase are less reactive than materials containing phosphorus in solid solution [11], and dissolution behaviour and bioactivity are decreased. It has still to be ascertained whether the behaviour of silicorhenanite (vs. HCA crystallization) is similar to the behaviour of rhenanite.

Finally, melting takes place in the 1070–1278 °C range. The two endothermic peaks on DTA thermograms are related to the melting of the two crystalline phases.

A summary of the transformations sequence is shown in Figure 12.

V. Conclusion

The bioactive glass 45S5 crystallizes principally in the $Na_2CaSi_2O_6$ phase rather than $Na_2Ca_2Si_3O_9$ in the 600–700 °C range. We suspect the existence of a new crystallized phosphate phase, $Na_2Ca_4(PO_4)_2SiO_4$.

After the glassy transition and before the crystallization process, a spinodal transformation of the glassy phase into two immiscible phases occurs, one phase rich in silicon and the other rich in phosphorus. We believe that the first one leads to the major crystalline phase and the second one to the crystalline phosphate phase.

The Rietveltd analyses showing the evolution of cell parameters in the major crystalline phase suggest that PO_4^{5-} groups enter the silica network during glass synthesis. At 800 °C, these groups are substituted by silica and lead to the crystalline phosphate phase.

Bioglass® crystallization kinetics show a rapid tendency of the material to crystallize. Furthermore, time–temperature–transformation curves were established which can be used to control the degree of crystallinity of porous blocks. We noticed, however, that these results cannot be extended to dense blocks.

Acknowledgements

The authors thank the Region Rhône-Alpes for its financial support.

References

[1] W. Cao and L.L. Hench, *Ceram Int* **22** (1996), pp. 493–507.
[2] L.L. Hench, R.J. Splinter, W.C. Allen and T.K. Greenlee, *J Biomed Mater Res Symp* **5** (1971), p. 117.
[3] T. Kokubo, *An Quím* **93** (1997), p. S49.
[4] V. Banchet, E. Jallot, J. Michel, L. Wortham, D. Laurent-Maquin and G. Balossier, *Surf Interface Anal* **36** (2004), pp. 658–665
[5] T. Kokubo, H. Kushitani and S. Sakka, *J Biomed Mater Res* **24** (1990), pp. 721–734
[6] L.L. Hench, *J Am Ceram Soc* **81** (1998) (7), pp. 1705–1728.

[7] H.A. El Batal, M.A. Azooz, E.M.A. Khalil, A. Soltan Monem and Y.M. Hamdy, *Mater Chem Phys* **80** (2003), pp. 599–609
[8] D.C. Clupper and L.L. Hench, *Biomaterials* **318** (2003), pp. 43–48.
[9] A. El Ghannam, E. Hamazawy and A. Yehia, *J Biomed Mater Res* **55** (2001), pp. 387–398.
[10] O. Peitl Filho, G.P. La Torre and L.L. Hench, *J Biomed Mater Res* **30** (1996), pp. 509–514.
[11] O. Peitl, E.D. Zanotto and L.L. Hench, *Biomaterials* **292** (2001), pp. 115–126
[12] J.M. Gomez-Vega, E. Saiz, A.P. Tomsia, G.W. Marshall and S.J. Marshall, *Biomaterials* **21** (2000) (2), pp. 105–111
[13] A.S. Rizkalla, D.W. Jones, D.B. Clark and G.C. Hall, *J Biomed Mater Res* **32** (1996), pp. 119–124.
[14] X. Chatzistavrou, T. Zorba, E. Kontonasaki, K. Chrissafis, P. Koidis and K.M. Paraskevopoulos, *Phys Stat Sol (a)* **201** (2004) (5), pp. 944–951.
[15] C.C. Lin, L.C. Huang and P. Shen, *J Non-Cryst Sol* (2005), pp. 1–9.
[16] Zenati R. Porous Bioglass and preparation thereof. French patent no. FR2005/001921, 2005.
[17] H. Oshato and I. Maki, *Acta Crystallogr C* **41** (1985), pp. 1575–1577.
[18] R.H. Doremus, Glass science, Wiley, New York (1994) p. 48.
[19] H. Rawson, Inorganic glass forming systems, Academic Press, New York (1967) p. 11.
[20] M.R. Filgueiras, G. La Torre and L.L. Hench, *J Biomed Mater Res* **27** (1993), pp. 445–453.
[21] E. Kontonasaki, T. Zorba, L. Papadopoulou, X. Chatzistavrou, K. Paraskevopoulos and P. Koidis, *Cryst Res Technol* **37** (2002), pp. 1165–1171.
[22] A. Clifford, R. Hill, A. Rafferty, P. Mooney, D. Wood and B. Samunera *et al.*, *J Mater Sci Mater Med* **12** (2001), pp. 461–469.
[23] A. Costantini, R. Fresa, A. Buri and F. Branda, *Thermochim Acta* **280/281** (1996), p. 237.
[24] S. Likitvanichkal and W.C. LaCourse, *J Mater Sci* **30** (1995), pp. 6151–6155.
[25] H. Ohsato, Y. Takeuchi and I. Maki, *Acta Crystallogr B* **46** (1990), pp. 125–131.
[26] N. Koga, J. Sestak and Z. Strnad, *Thermochim Acta* **203** (1992), pp. 361–372.
[27] P.W. McMillan In: J.P. Roberts and P. Popper, Editors, *Glass ceramics* (2nd ed.), Academic Press, New York (1979), p. 76.
[28] K.J. Elgayar, A.E. Aliev, A.R. Boccaccini and R.G. Hill, *Journal of Non-Crystalline Solids* **351** (2005), pp. 173–183.
[29] M. Holand, A. Dommann, W. Holand, E. Apel and V. Rheinberger, *Glass Sci Technol* **78** (2005) (4), pp. 153–158.

Acta Materiala, 2007, 55(10), 3305-3313, doi:10.1016/j.actamat.2007.01.029

Figures

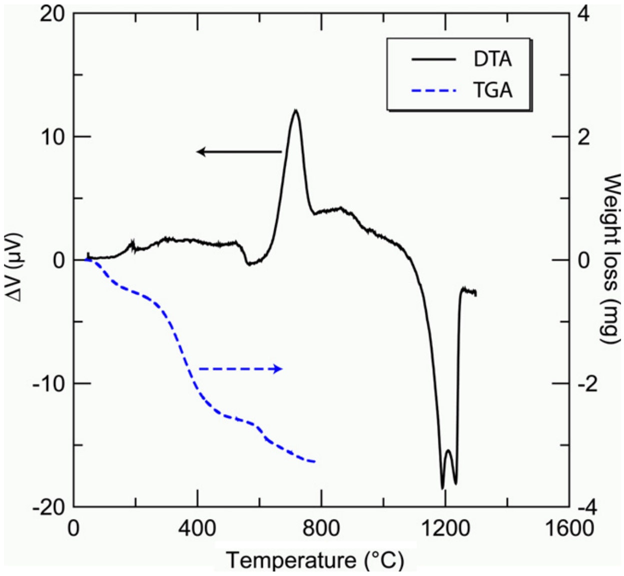

Figure 1: TGA–TDA of 45S5 Bioglass®.

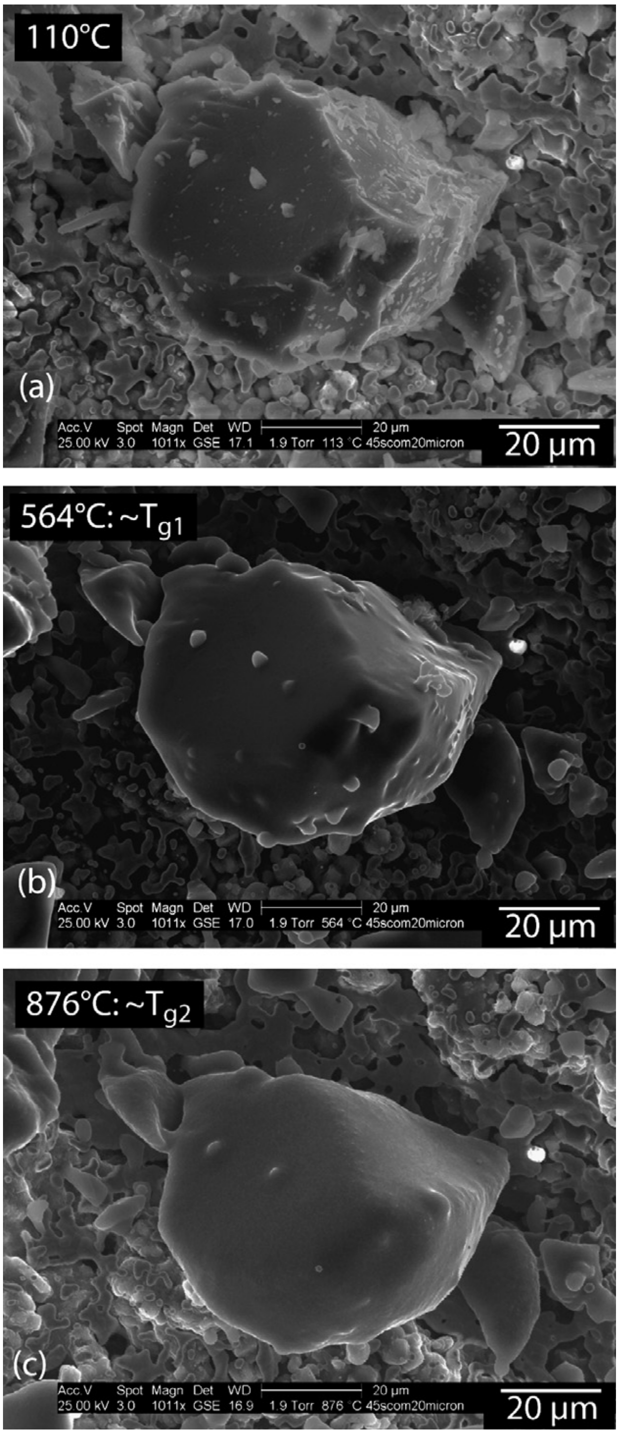

Figure 2: ESEM micrographs taken at low magnification on one Bioglass® grain during in situ heating from room temperature to 950 °C. Three micrographs have been selected to show the evolution of grain morphology with temperature: 110 °C (a), around T_{g1} = 550 °C (b) and T_{g2} = 850 °C (c).

Acta Materiala, 2007, 55(10), 3305-3313, doi:10.1016/j.actamat.2007.01.029

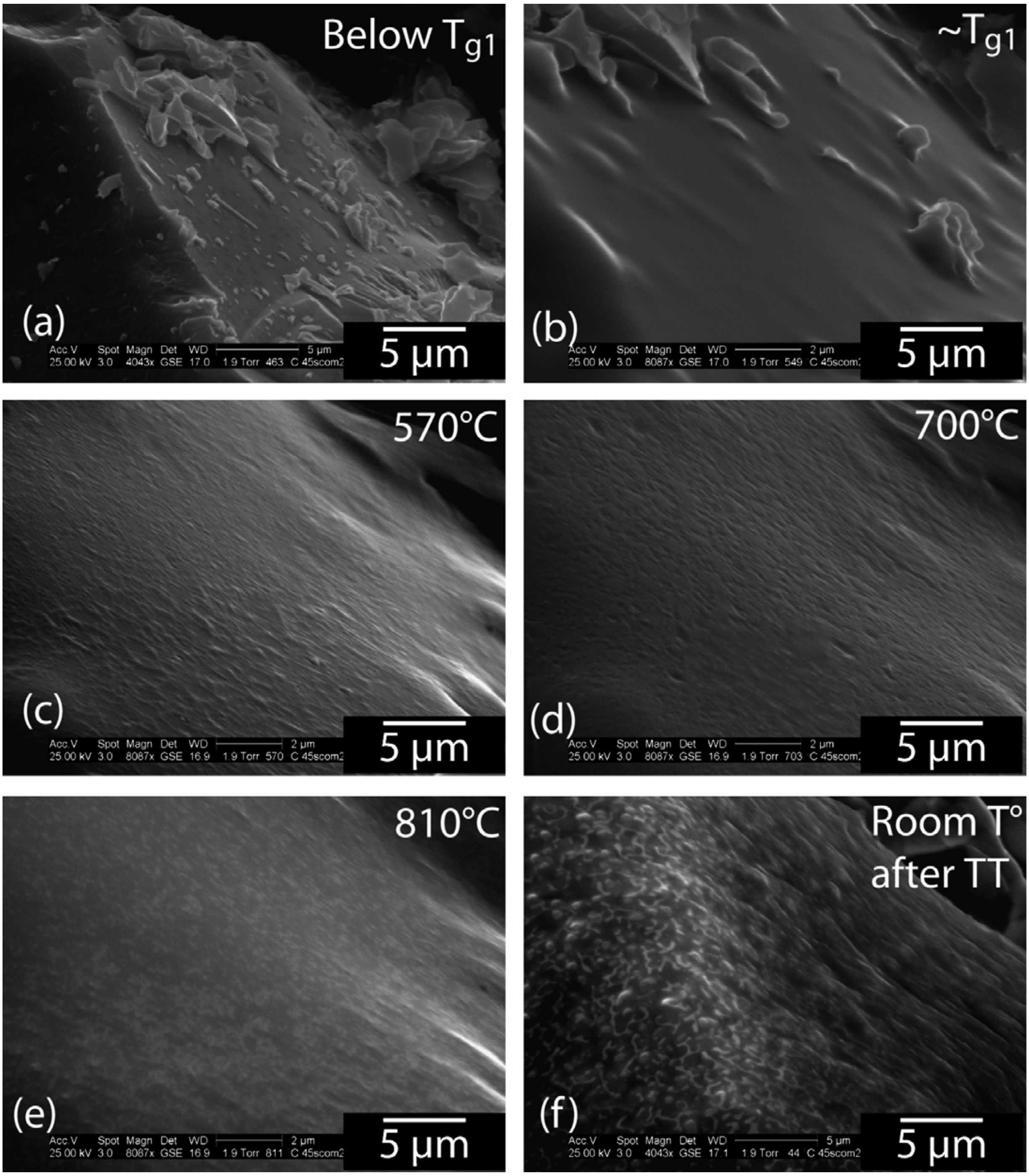

Figure 3: ESEM micrographs taken in situ at higher magnification at the surface of the same grain. (a) Below T_{g1}. (b) At T_{g1} = 550 °C. (c) An additional event is observed at T_s = 570 °C, prior to crystallization, which was not observed on the DTA thermograms. The surface, which was completely smooth after the glassy transition, presents a specific morphology, with the creation of domains. (d) The result of crystallization, taken at 700 °C, with the formation of "craters" at the surface. (e) At 800 °C, migration of a second phase with a different morphology and structure. (f) Surface after thermal treatment at 950 °C (the micrograph was taken at ambient temperature, after cooling, to ensure thermal stability and better contrast and resolution).

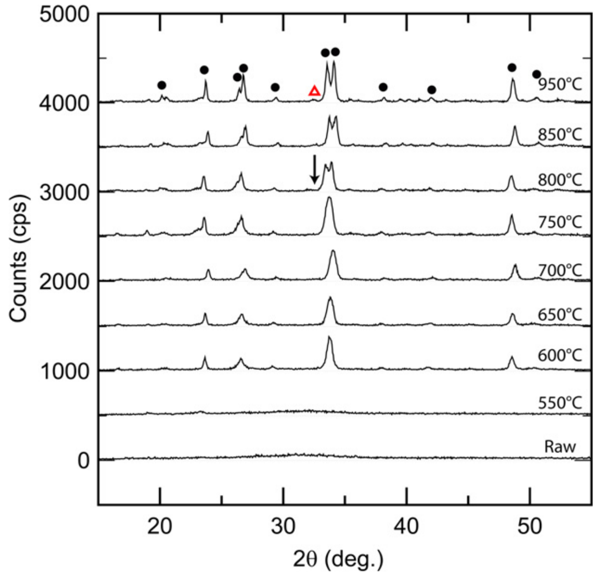

Figure 4: Diffractograms of raw and thermally treated bioactive glass 45S5. Under 600 °C the Bioglass® remains amorphous. Over this temperature, crystallization takes place by the formation of $Na_2CaSi_2O_6$ (•: PDF 77–2189). At 800 °C, the two major peaks of this phase begin to be dissociated while the crystallization of silicorhenanite (▲: PDF 32–1053, isostructural to apatite) begins. At 1050 °C, the material begins the melting process).

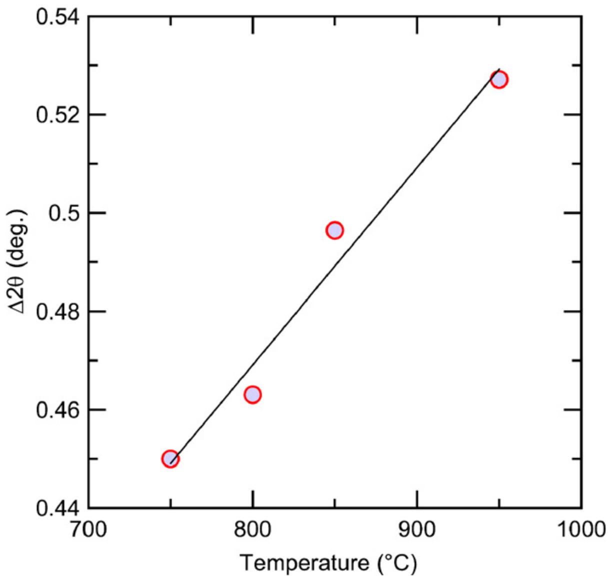

Figure 5: Separation (Δ2θ) of the two peaks of major intensity of $Na_2CaSi_2O_6$ as a function of temperature. A linear dependency is observed.

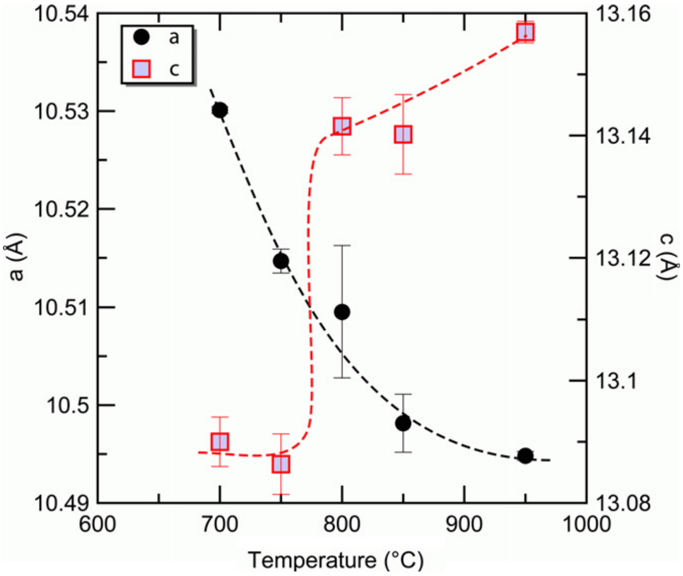

Figure 6: Rietveltd refinement applied to the different diffractograms from 750 to 950 °C to measure the lattice parameters (a and c).

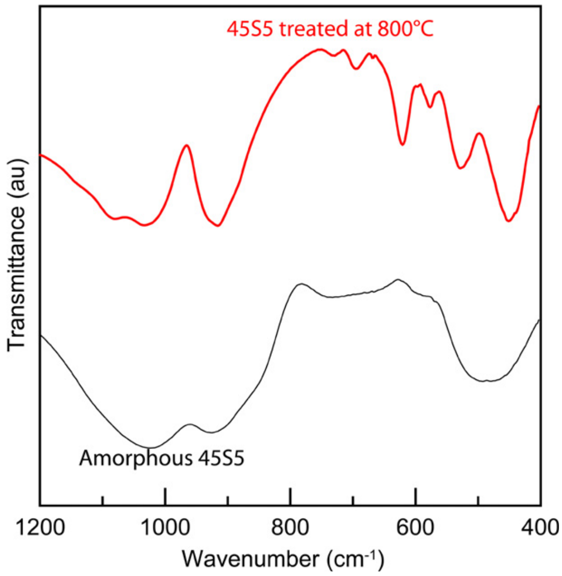

Figure 7: FTIR spectra taken on the powder before and after thermal treatment at 800 °C.

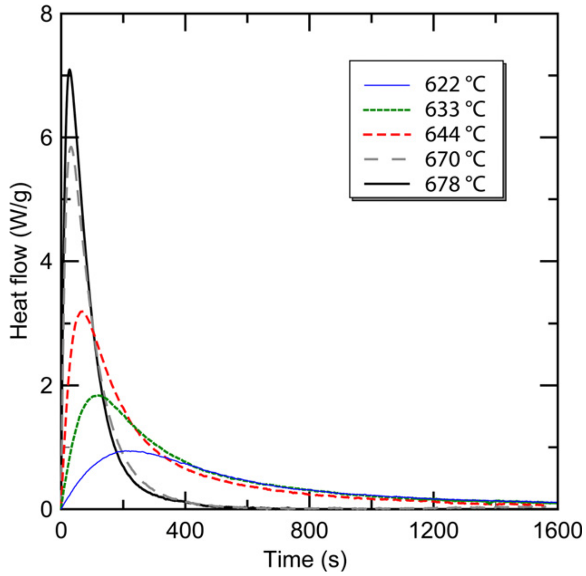

Figure 8: Isothermal crystallization peaks obtained by DSC at different temperatures.

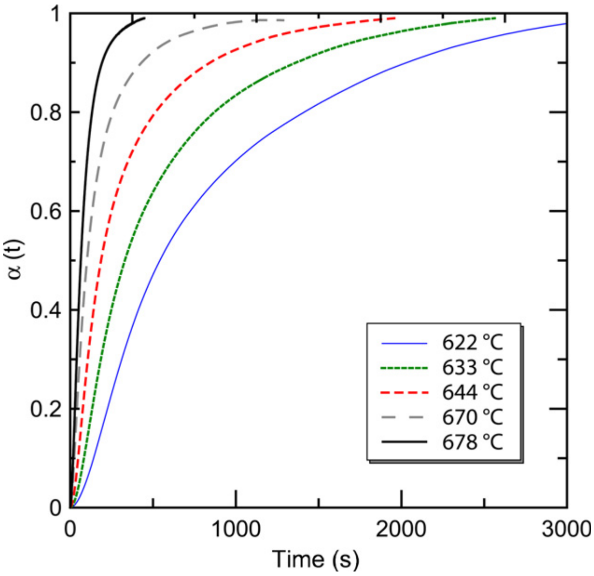

Figure 9: Plot of $\alpha_T(t)$ vs. time obtained from the DSC measurements and from Equation (2).

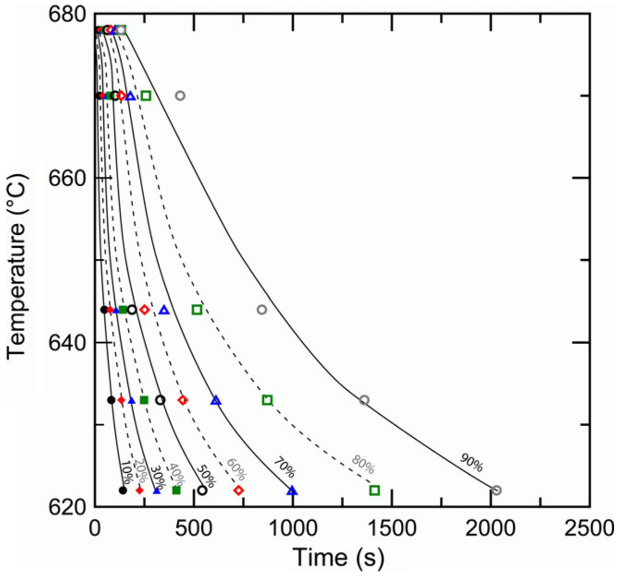

Figure 10: TTT curves of 45S5 Bioglass®.

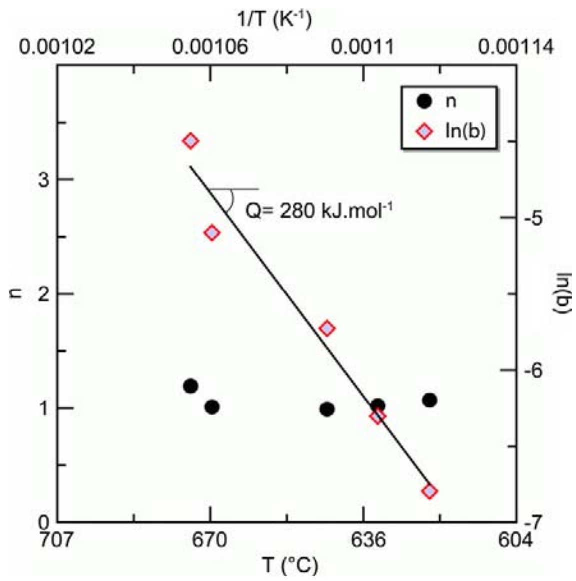

Figure 11: Values obtained for n and ln(b) for each temperature.

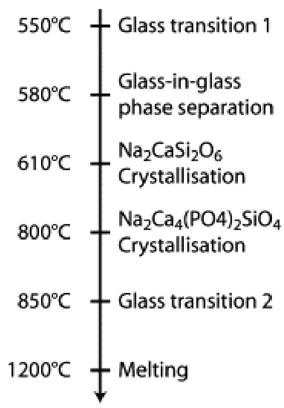

Figure 12: Summary of the structural transformations of 45S5 with temperature.

Tables

Table 1: $Na_2CaSi_2O_6$ crystal size evaluated from XRD, calculated from Equation (1)

Temperature (°C)	650	750	800	850	950
Crystal size (nm)	18	15	36	35	41